How do different pathways connect the stratospheric polar vortex to its tropospheric precursors?

Raphael H. Köhler[1,*], Ralf Jaiser[1,*], and Dörthe Handorf[1]

[1]Alfred Wegener Institute, Helmholtz Centre for Polar and Marine Research, Potsdam
[*]These authors contributed equally to this work.

Correspondence: Raphael Köhler (Raphael.Koehler@awi.de), Ralf Jaiser (Ralf.Jaiser@awi.de)

Abstract. Processes involving troposphere–stratosphere coupling have been identified as important contributors to an improved subseasonal to seasonal prediction in mid-latitudes. However, there is only a very vague understanding of the localised coupling mechanisms and involved timescales, in particular when it comes to connecting tropospheric precursor patterns to the strength of the stratospheric polar vortex. Based on a novel approach in this study, we use ERA5 reanalysis data and ensemble

5   simulations with the ICOsahedral Non-hydrostatic atmospheric model (ICON) to investigate tropospheric precursor patterns, localised troposphere–stratosphere coupling mechanisms and the involved timescales of these processes in Northern Hemisphere extended winter. We identify two precursor regions: Mean sea level pressure in the Ural region is negatively correlated to the strength of the stratospheric polar vortex for the following 5–55 days with a maximum at 25–45 days, and the pressure in the extended Aleutian region is positively correlated to the strength of the stratospheric polar vortex the following 10–50

10   days with a maximum at 20–30 days. A simple precursor index based on the mean pressure difference of these two regions is very strongly linked to the strength of the stratospheric polar vortex in the following month. The pathways connecting these two regions to the strength of the stratospheric polar vortex, however, differ from one another. Whereas a vortex weakening can be connected to prior increased vertical planetary wave forcing due to high-pressure anomalies in the Ural region, this is not the case for the extended Aleutian region. A low-pressure anomaly in this region can trigger a Pacific/North American

15   (PNA) related pattern leading to geopotential anomalies of the opposite sign in the mid-troposphere over central North America. This positive geopotential anomaly travels upward and westward in time directly penetrating into the stratosphere and thereby strengthening the stratospheric Aleutian High, a pattern linked to the displacement towards Eurasia and subsequent weakening of the stratospheric polar vortex. Overall, this study emphasises the importance of the non-zonally-averaged picture for an in-depth understanding of troposphere–stratosphere coupling mechanisms. Additionally, this study demonstrates that

20   these coupling mechanisms are realistically reproduced by the global atmosphere model ICON.

1 Introduction

Seasonal predictability is based on processes that evolve on slower timescales than the synoptic systems of the troposphere. These processes include slow changes in the lower boundaries, such as soil humidity, snow cover, or ocean temperatures, but also the evolution of the stratospheric polar vortex throughout winter. Based on the interactions between planetary and synoptic

25 scales on timescales of some days to multiple weeks, the coupling between stratosphere and troposphere has been identified as an important source of predictability for a range of processes on subseasonal to seasonal timescales in mid-latitudes in winter (Domeisen et al., 2020a). However, seasonal prediction can only benefit from the slower evolution of stratospheric processes if we develop an in-depth understanding of the involved coupling mechanisms with the troposphere. Moreover, models used for seasonal prediction need to be able to reproduce these processes.

30 By using the Northern Annular Mode (NAM) to characterise the polar vortex already Baldwin and Dunkerton (2001) showed that large variations in the strength of the stratospheric circulation are often followed by anomalous tropospheric weather regimes for up to 60 days. The downward propagation of stratospheric anomalies and the effects on surface patterns have been studied thoroughly since then, in particular, for the most dramatic stratospheric phenomenon, the Sudden Stratospheric Warmings (SSW) (e.g. Charlton-Perez et al., 2018; Afargan-Gerstman and Domeisen, 2020; Baldwin et al., 2021; Butchart, 2022).

35 This downward response is well reproduced in model studies and is known to potentially contribute to surface predictability (e.g. Scaife et al., 2016; Domeisen et al., 2020a). But how well can stratospheric extreme events be predicted in advance? Karpechko (2018) shows that the ECMWF Extended-Range Forecast System is able to predict SSWs with high probability at lead times of 12–13 days. Overall, the stratosphere exhibits a slower growth of the signal-to-noise problem as compared to the troposphere, and thus, even allows for predictability beyond 2 weeks (Domeisen et al., 2020b). However, stratospheric

40 extreme events themselves tend not to be predictable beyond deterministic timescales and in particular, SSW events tend to be less predictable.

Based on the early studies of Matsuno (1971) on the role of enhanced tropospheric wave forcing in triggering SSWs, different studies have investigated tropospheric precursor patterns to potentially increase the range of stratospheric predictability. Many studies thereby focus on the Ural blocking pattern as part of a wave-1 anomaly as a precursor pattern for SSWs (e.g. Garfinkel

45 et al., 2010; Cohen and Jones, 2011). Moreover, this blocking pattern has recently received additional attention, as it plays an important role in dynamically linking Arctic amplification and sea ice loss to changes in mid-latitude circulations patterns via a robust but highly intermittent stratospheric pathway (Jaiser et al., 2016; Hoshi et al., 2019; Cohen et al., 2020; Siew et al., 2020; Jaiser et al., 2023): The strong reduction of Arctic sea ice in autumn and winter, in particular in the Barents and Kara seas, and the associated heating of the overlying atmosphere favour more frequent blocking-type ridges over northwestern

50 Eurasia in early winter, which facilitate the enhanced propagation of wave energy into the stratosphere, where wave breaking can lead to a disruption of the stratospheric polar vortex (Overland et al., 2016; Crasemann et al., 2017). A further potential precursor pattern, namely pressure anomalies in the North Pacific region, has received less attention in literature focusing on precursor patterns of SSWs (e.g. Baldwin et al., 2021). However, Bao et al. (2017) identify the positive phase of the Pacific-North American pattern (PNA) as a precursor of SSWs by means of constructive interference with the climatological planetary

55 wave-1 pattern. Whereas the Ural blocking plays an important role in Arctic–midlatitude linkages, the Aleutian Low and the PNA have been identified as a pathway connecting the tropical phenomenon El Niño Southern Oscillation (ENSO) to the strength of the stratospheric polar vortex in winter (e.g. Domeisen et al., 2019).

Kretschmer et al. (2017) show that there is a large potential in identifying precursor mechanisms, as they are able to correctly predict 46% of the extremely weak stratospheric polar vortex states for lead times of 16–30 days using a linear regression

60 prediction model based on causal precursors. However, most previous studies average their signals over fixed lag times. Thus, information on the exact timescales of the coupling mechanisms is lost. Based on this, one objective of this paper is to investigate tropospheric precursors of the stratospheric circulation in winter, including a careful analysis of the involved timescales, patterns, and mechanisms. In contrast to earlier studies, we moreover not only focus on SSWs but on precursor patterns of stratospheric circulation by means of the NAM. Thereby, we evaluate the tropospheric precursor patterns and quantify the

65 involved timescales in Sect. 3.1. Moreover, a strong focus lies on the mechanisms and processes involved in coupling tropospheric pressure anomalies to stratospheric circulation changes. Thus, in Sect. 3.2 we investigate the coupling pathways with a novel time and space-resolved method. By comparing results from reanalysis data to ensemble simulations with the global ICOsahedral Non-hydrostatic atmospheric model (ICON), we furthermore test how these troposphere–stratosphere coupling processes are represented in ICON. The ensemble approach in ICON additionally helps us to better quantify the signal-to-noise

70 ratio.

2 Data and methods

2.1 Data

In this study, we use daily and monthly mean ERA5 reanalysis data (Hersbach et al., 2020) for the period 1979 to 2021. The reanalysis furthermore serves as a reference for the ensemble simulations with the atmospheric general circulation model

75 ICON (Zängl et al., 2015) version 2.1.0. The model is run with the horizontal resolution R2B5, which corresponds to a grid mesh of approximately $80\,\mathrm{km}$, and with 90 vertical levels up to a height of $75\,\mathrm{km}$. The ICON climatology is created by simulating periods from September to May for the years 1979/80 to 2016/17 (38 years), and each period is simulated by five ensemble members. Thus, yielding a total of 190 nine-month simulations. The ensemble members were generated by shifting the initialisation by $\pm 6\,\mathrm{h}$ and $\pm 12\,\mathrm{h}$. We prescribe mid-monthly sea surface temperatures and sea ice concentrations produced

80 by the Program for Climate Model Diagnosis and Intercomparison for the Atmosphere Model Intercomparison Project (AMIP) experiments of CMIP6 (Durack and Taylor, 2018). Based on the results of Köhler et al. (2021), we use a tuned setup of the subgrid scale orographic (SSO) drag and the non-orographic gravity wave drag scheme, as in particular the stratospheric polar vortex shows a more realistic behaviour. The ICON simulations we use in this study are well tested and correspond to the ICON_{gwd-} experiment of Köhler et al. (2021).

85 ### 2.2 Methods

The basic mean of quantifying the strength of the stratospheric polar vortex in this study is the Northern annular mode (NAM), which is the dominant pattern of dynamic variability in the extratropical Northern Hemisphere (NH). Based on Baldwin and Thompson (2009), we use the empirical orthogonal function (EOF) of the daily, zonally-averaged geopotential at each pressure level to calculate the NAM. It is represented by the first principle component of this EOF. Weak (strong) stratospheric

polar vortex events are defined by the 20th (80th) percentile of the NAM at 10 hPa. The statistical significance of composite differences in this study is assessed with a two-sided, nonparametric Wilcoxon-test (Bauer, 1972; Hollander et al., 2013).

The influence of tropospheric anomalies on the stratospheric circulation is characterised by vertical wave propagation following Plumb (1985). The Plumb Flux is calculated from perturbations defined as deviations from the 91-day rolling mean annual cycle of the full ERA5 data or full ICON ensemble, respectively. We consider only low-frequency or large-scale contributions to the Plumb Flux and therefore apply a low-pass filter sensitive to timescales above 10 days (Blackmon and Lau, 1980) to the perturbations. In this study, we are interested in localised contributions to the vertically propagating wave activity and therefore only analyse the vertical component of the Plumb flux.

To be able to analyse our data in time and space, we have to reduce the dimensionality. Therefore, we implement meridional averaging typically from 45°N to 80°N. During the testing of our methods, we varied this region over Northern Hemisphere extratropical latitude bands with no contradictions found. This keeps the temporal, longitudinal, and vertical dependence as variable arguments in the subsequently described analytical methods.

A regression analysis is performed between a time-shifted dependent variable and an independent variable that is averaged on 10° longitude bins. The daily values of the independent variable are taken from all days of the given month from all years and all ensemble members if applicable. The corresponding diagram shows the regression coefficient that results from anomalies of the independent variable at a given longitude along the x-axis and the dependent variable shifted by days given along the y-axis relative to the independent variable. Regression coefficients with a p-value above 0.05 are considered non-significant and are displayed as hatched areas provided that the null hypothesis is that the slope is zero, using Wald Test (Wald, 1943) with t-distribution of the test statistic. Areas with p-values below 0.001 are additionally encircled.

This concept of regression analysis is extended into three dimensions. Here, the independent variable is a daily index of a given variable at a given position from a given month. The dependent variable is varied along the x-axis for its longitudinal position and shifted in time relative to the index along the y-axis. Additionally, the z-axis shows the vertical dependency on pressure. Both input data have been detrended prior to analysis. The diagram then shows the location of the 10% largest absolute correlation coefficients between index and dependent variable. These have been verified to easily exceed a 0.001 significance test as described before in terms of the regression analysis.

3 Results

## 3.1 Tropospheric precursor patterns and timescales

The main focus of this section lies in identifying tropospheric precursors of anomalous stratospheric NAM and thereby quantifying the involved timescales. The stratospheric polar vortex exhibits its largest variability in January when on the one hand the daily mean, zonal mean westerlies (in 60°N and at 10 hPa) of an undisturbed vortex can reach up to 70 m/s, and on the other hand can reverse allowing for easterlies of more than 20 m/s during vortex breakdowns. Moreover, more frequent Ural-blockings in December and subsequently a weakened stratospheric vortex in January have been identified as important parts of the stratospheric pathway linking Arctic amplification to stratospheric circulation (e.g. Jaiser et al., 2016; Crasemann et al.,
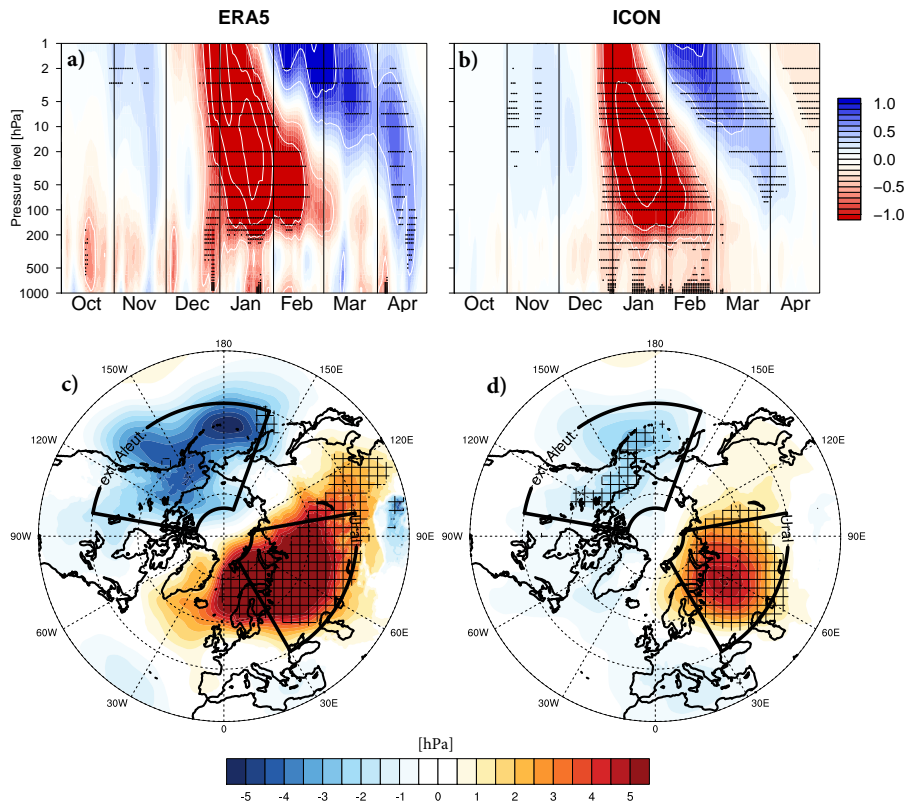
Figure 1. Composites of the time–height development of the NAM for weak stratospheric vortex states based on the 20th percentile of the January mean NAM at 10 hPa in ERA5 (a) and ICON (b). The NAM index is nondimensional. The contour interval for the white contours is 0.5. Note that due to common practice negative values (weak NAM) are red and positive values (strong NAM) are blue. Composites of the December mean sea level pressure (MSLP) in hPa for the same January weak vortex events in ERA5 (c) and ICON (d). The Ural region and the extended Aleutian region are marked by black boxes. The definitions of the regions are based on the analysis of Fig. 2. Stippling in a-d indicates statistical significance at the 95% level according to a two-sided Wilcoxon-test.

2017). Based on this, we will start our analysis focusing on stratospheric polar vortex strength in January. However, later in the manuscript, we will show that our key findings stay the same for the months of November, December, February, and March 125 (e.g. Fig. 3).

Independent of the type of definition, weak vortex events tend to have a rather typical pattern of downward propagation, which was first described by Baldwin and Dunkerton (2001) and is often referred to as "dripping paint" plot. Figures 1 a) and b) recreate these famous time–height cross sections, however, for January weak vortex events only. These events are defined by the 20th percentile of the monthly mean NAM index at 10 hPa in January, yielding 9 events in ERA5 and 40 events in 130 ICON. The larger amount of events due to the ensemble approach explains why the overall signals are smoother in ICON. After the onset of negative NAM signals in the upper stratosphere in late December, the signals propagate downward and
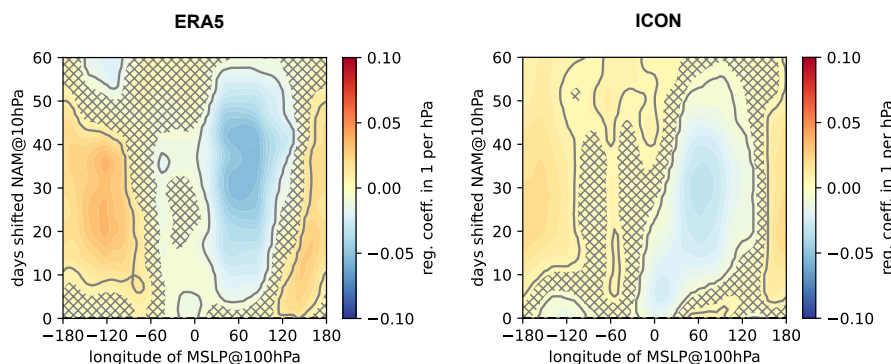
Figure 2. Regression of 45°N to 80°N meridional mean MSLP onto the 10 hPa NAM. MSLP is averaged over 10° longitude bins with their respective center positions given along the x-axis. Daily values of MSLP from December of ERA5 data (a) and all years and ensemble members of ICON data (b) are used. Data of the 10 hPa NAM is shifted by days given on the y-axis relative to MSLP data. Areas with regression coefficients with p-values above 0.05 are hatched, and areas with p-values below 0.001 are encircled.

remain present in the lower stratosphere throughout January and February. Some of the weak stratospheric NAM signals also propagate to the troposphere leading to a weakening of the tropospheric NAM. The tropospheric signals are larger towards the surface, which is described as "surface amplification" and is caused by reinforcing tropospheric near-surface processes (Baldwin et al., 2019, 2021). On average, weak vortex events in January are preceded (November) and followed (February and March) by a significantly stronger upper stratospheric polar vortex. ICON is able to reproduce the basic known features of weak stratospheric vortex events in January, also including a realistic downward propagation as well as the upper stratospheric strengthening before and after the event. Although the negative NAM anomalies overall propagate downwards starting in late December, there are also some indications of tropospheric precursor signals in December in ERA5 and ICON. Even when using a very ordinary composite approach for years with a weak stratospheric vortex in January (cf. Fig. 1 c and d), the known mean sea level pressure (MSLP) precursor patterns become visible in December: A significant high-pressure anomaly over northwestern Eurasia centered over the Ural mountains, and a low-pressure anomaly over the Northern Pacific, centered around the Aleutian islands and Alaska. The anomaly patterns are known to constructively interfere with the climatological wave-1 pattern in the troposphere (e.g. Bao et al., 2017).

Figure 2 offers a more conceptual view of the connection between tropospheric pressure patterns in December and strato-spheric NAM in the following, thereby moreover allowing for an estimation of the involved timescales. The meridional mean MSLP from 45°N to 80°N in December (x-axis) is regressed onto the NAM at 10 hPa (y-axis) using daily mean ERA5 reanal-ysis and ICON ensemble data. Figure 1 shows that December sea level pressure is a predictor for the NAM at 10 hPa, and once again there are two areas that stand out: An area of significant negative regression centered over the Ural region and an area of positive regression in the sphere of influence of the Aleutian low extending from the Sea of Okhotsk to the Rocky Mountains. The negative regression over the Ural region is strongest at about 60°N and with a lag of 25–45 days, indicating that high (low) pressure in this region is connected to a weakening (strengthening) of the stratospheric polar vortex with approximately
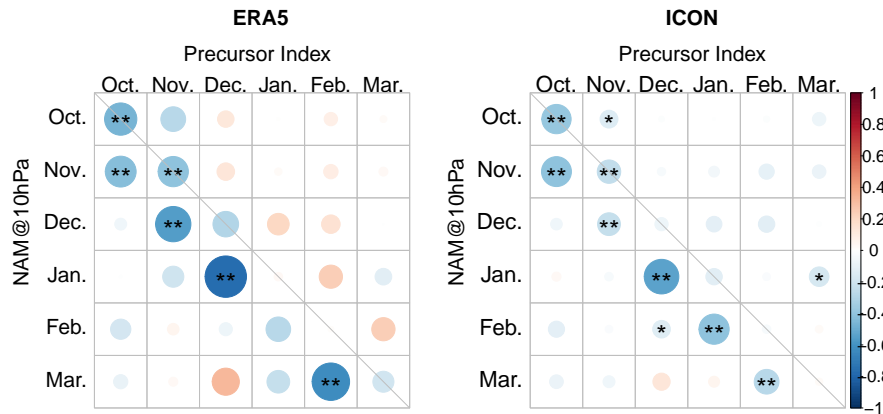
Figure 3. Spearman correlation between the detrended, monthly mean precursor index and NAM index at 10 hPa. Circle size and colour correspond to the strength of the correlation coefficients. Blue (red) colours denote a negative (positive) correlation and the stars denote significance, with one star indicating statistical significance at the 95% level and two stars statistical significance at the 99% level.

one month lag. The maximum of the positive regression is centered over the Rocky Mountains with a lag of 20–30 days, thus indicating that low (high) pressure anomalies in the extended Aleutian low area are connected to a weakening (strengthening) of the stratospheric polar vortex. The regions of interest are in accordance with the precursor patterns depicted in Fig. 1. Both patterns show significant signals already after a few days and last for around 50 days. ICON reproduces the described patterns, with a maximum negative regression at a lag of 30 days, and a maximum positive regression at 20–30 days lag. However, the maximum of the positive regression is shifted towards the antimeridian and thus the climatological position of the Aleutian Low. Based on Fig. 2, we create a straightforward precursor index (PI), which is defined by the detrended pressure difference between the Ural and the extended Aleutian area. The Ural region is defined by the average MSLP in 45°N–80°N and 30°E–100°E, and the extended Aleutian region is defined by 45°N–80°N and 160°E–100°W.

Figure 3 makes use of this precursor index and visualises the Spearman correlation coefficients between the monthly mean precursor index and the monthly mean NAM index at 10 hPa. The strong and highly significant negative correlation between the December precursor index and the January NAM at 10 hPa confirms the previous results. It indicates that a high (low) precursor index in December favours a weak (strong) stratospheric NAM in January. The precursor index is high when there is a high-pressure anomaly in the Ural region and/or a low-pressure anomaly in the extended Aleutian area. The correlation between the December surface index and January stratospheric index shows the largest correlation coefficient of the possible combinations with a coefficient of 0.76 in ERA5 and 0.54 in ICON. However, the precursor index based on MSLP solely also works as a predictor for the stratospheric NAM in all other extended winter months from November to March, with the only exception for February, when the negative correlation between January precursor index and February NAM is not statistically significant in the ERA5 data, but highly significant in the ICON ensemble simulations. Overall, ICON reproduces the signals from ERA5 very well, with slightly smaller correlation coefficients but higher statistical significance due to the higher amount
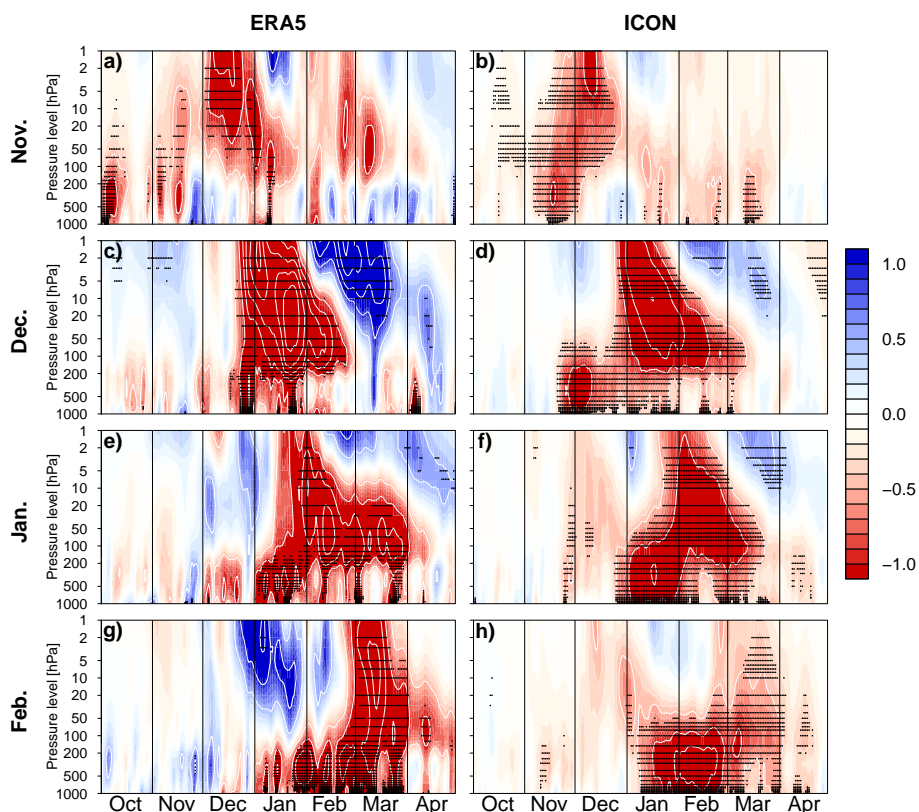
Figure 4. Composites of the time–height development of the NAM for the difference between high (80th percentile) and low (20th percentile) precursor index in ERA5 (a,c,e,g) and ICON (b,d,f,h). The composites are created based on the monthly mean precursor index for the months November (a,b), December (c,d), January (e,f) and February (g,h). The NAM index is nondimensional. The contour interval for the white contours is 0.5 and stippling indicates statistical significance at the 95% level according to a two-sided Wilcoxon-test. Note that due to common practice negative values (weak NAM) are red and positive values (strong NAM) are blue.

of realisations. Interestingly, the connection between the MSLP anomalies and the stratospheric circulation seems to be more direct in October and November, as there is already a significant negative correlation without a time lag, which disappears during late winter. The two components of the precursor index were also analysed individually and although the Ural pressure patterns contribute more strongly to the correlation with stratospheric NAM of the following month, subtracting the averaged MSLP of the extended Aleutian area gives a clear added value, in particular in late winter.

The potential of the precursor index in the context of seasonal prediction is demonstrated in Fig. 4, which shows NAM composite differences between years with a high and a low precursor index in the months November (a,b), December (c,d), January (e,f) and February (g,h) for ERA5 and ICON. The anomalies in the precursor index already tend to manifest as a tropospheric NAM signal, which propagates into the stratosphere by the end of the month. A high (low) precursor index is clearly connected to a negative (positive) NAM signal. Although the precursor index is based solely on MSLP patterns, strong

stratospheric circulation anomalies become visible in the two months following the original precursor anomaly. Moreover, these stratospheric anomalies propagate back into the troposphere leading to significant tropospheric NAM signals for up to 3 months after the original anomaly in the precursor index. Even though the basic patterns of NAM propagation are similar for the four displayed months, there are some distinct features subject to the month of the original precursor anomaly: An anomalous precursor index in November is connected to significant tropospheric NAM anomalies in the same month, but first NAM signals are already visible in October. These signals in late autumn tend to directly propagate into the stratosphere, which is in line with the results from Fig. 3. The strongest NAM signals manifest in the upper stratosphere in December, followed by a downward propagation into the lower stratosphere in January. This is also when the stratospheric signals tend to propagate back into the troposphere, thereby significantly affecting tropospheric circulation. The ICON ensemble simulations reproduce this pattern with slightly weaker intensity. However, also suggesting a more persistent influence on the tropospheric circulation also in February and March. In December, the stratospheric response to the precursor index in ERA5 and ICON is strongest, once again in accordance with Fig. 3. The strong negative NAM signal in January and February is followed by a significant positive NAM anomaly in the upper stratosphere in February, and in the lower stratosphere in spring. Precursor anomalies in January are connected to very strong tropospheric NAM signals in the same month. These propagate into the stratosphere in late January, leading to strong downward propagating signals affecting the lower stratosphere in February and March. The influence on the upper and mid stratosphere only lasts until mid-February in ERA5, thus explaining why the correlation between the monthly mean precursor index in January and the monthly mean NAM at 10 hPa in February is weaker and not significant (cf. Fig. 3). However, the effect on the lower stratosphere is strong and highly significant. This once again impacts the troposphere yielding highly significant signals in February and March in ERA5 and ICON. A strong precursor index in February is connected to a negative tropospheric NAM in January and February. This signal then propagates into the stratosphere in late February and early March leading to a significant weakening of the stratospheric polar vortex in March and April, including the known "dripping" events into the troposphere. Overall, the NAM patterns clearly demonstrate that there can be strong coupling between the troposphere and the stratosphere in NH extended winter and that a better understanding of the involved mechanisms could help to improve subseasonal to seasonal prediction. Hence, in the following chapter, we focus on these coupling mechanisms, in particular on the upward propagation of tropospheric anomalies into the stratosphere.

3.2 Coupling mechanisms

The previous section demonstrated that the precursor index based on MSLP variations in the Ural and extended Aleutian area is strongly connected to the stratospheric circulation in the following two months. Yet, although there is this clear connection, the actual processes involved in coupling remain unclear and shall be investigated in this section.

Based on planetary wave theory of Matsuno (1971), we initially investigate the role of tropospheric wave forcing in coupling the troposphere and stratosphere. Vertical wave propagation is quantified by means of the Plumb Flux (Plumb, 1985) as described in Sect. 2.2. As a first step, we investigate if changes in the precursor index are related to local anomalous wave activity flux above the tropopause. Therefore, Fig. 5 depicts the monthly mean Plumb flux composite differences between months with a high and months with a low precursor index as a function of longitude. Each month is a separate composite based on the
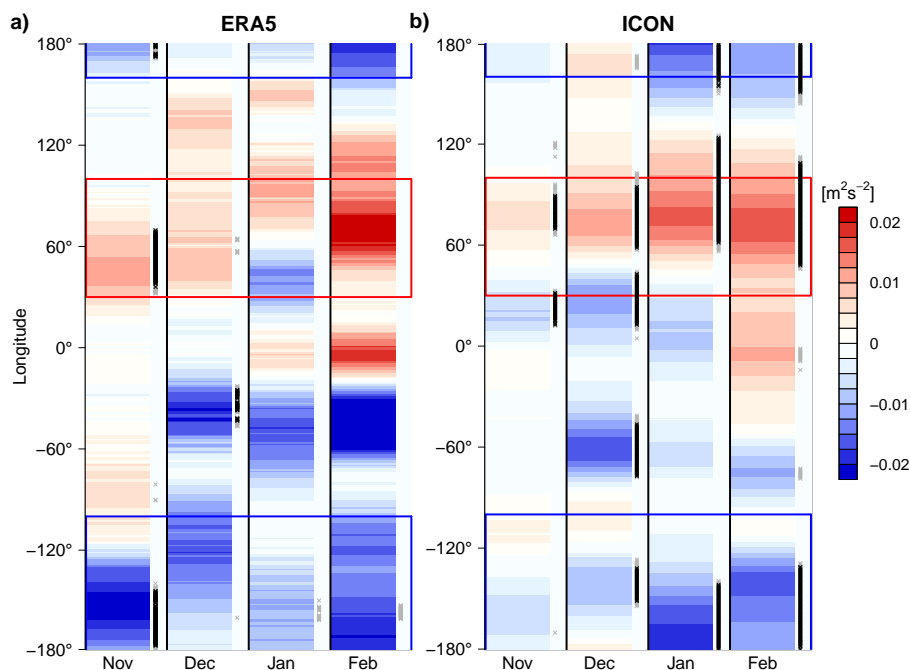
Figure 5. Composites of the monthly and 45°N to 80°N meridional mean vertical component of the Plumb flux at 100 hPa as a function of longitude for the difference between high (80th percentile) and low (20th percentile) precursor index events in ERA5 (a) and ICON (b). The composites are created based on the monthly mean precursor index for the months November, December, January and February separately. Black (grey) stars indicate statistical significance at the 95% (90%) level according to a two-sided Wilcoxon-test. The red and the blue box mark the Ural and extended Aleutian region, which are used to calculate the precursor index based on MSLP.

monthly mean precursor index. There is some indication that the monthly mean precursor index is connected to anomalous meridional mean Plumb flux at 100 hPa, with predominantly positive anomalies in the Ural region (red box) and predominantly negative anomalies in the extended Aleutian region (blue box). The MSLP difference in these two regions was used to calculate the precursor index (cf. previous section). Thus indicating that a high precursor index (high MSLP over Ural region and/or low MSLP over extended Aleutian region) can, on the one hand, contribute to additional wave activity flux into the stratosphere at longitudes varying around 70°E, and, on the other hand, contribute to reduced flux into the stratosphere at longitudes varying around 160°W. These longitudes coincide with the regions that were used to define the precursor index. There does not seem to be a large time lag between the precursor index and the Plumb flux, as the signals in the respective following month are smaller (not shown). Whereas in November the signals in ERA5 show higher significance and are centered over the respective region, the main signals in December to February are less significant. This could however be related to the small number of events and the large internal variability of stratospheric processes, in particular in mid and late winter. The ICON results support this perception, as the basic patterns with a predominantly negative relation between the precursor index and the Plumb flux in the

Western Hemisphere, and a predominantly positive relationship between the precursor index and the Plumb flux in the Eastern
230　Hemisphere are reproduced, and are significant, in particular in the Ural and Aleutian region.

But how does the Plumb flux relate to the strength of the stratospheric polar vortex by means of the NAM? Instead of using
MSLP as a function of longitude as in Fig. 2, we regress the 45°N to 80°N meridional mean Plumb flux at 100 hPa onto the
10 hPa NAM in Fig. 6. The Plumb fluxes are shown as a function of longitude and the NAM index as a function of days.
The connection between wave activity in 100 hPa and the stratospheric polar vortex is not as straightforward as one might
235　expect, as increased Plumb flux does not necessarily imply a weakening of the stratospheric polar vortex. The relation between
Plumb flux and the NAM at 10 hPa is highly dependent on the longitude and month in question. In particular in November
and December, there is a significant band of negative regression coefficients which indicates that increased (decreased) Plumb
fluxes from approximately 60°E to 130°E are connected to a weaker (stronger) NAM with a lag of 0 to 60 days (cf. Fig. 6 a-d).
This relationship is weakened and shifted westward in January and February in ERA5, a feature that is only partly reproduced
240　by the ICON ensemble. That being said, additional Plumb flux can also be followed by a strengthened NAM. This positive
regression can be mainly observed in the Western Hemisphere. It however cannot fully explain the strong link between the
MSLP in the extended Aleutian area and the strength of the NAM (cf. Fig. 2), as the signals are weak and patchy. Overall, there
is some explanatory power in the Plumb fluxes linking MSLP patterns to stratospheric circulation via increased (decreased)
Plumb fluxes in the Ural (Aleutian) area during strong precursor events (cf. Fig. 5), followed by a negative relation between
245　the Plumb flux and the NAM in the Ural region. However, this classic approach using the Plumb wave activity flux does not
seem sufficient to explain the strong lagged linkage between the troposphere and stratosphere, in particular for the extended
Aleutian region.

Based on this, we want to introduce an exploratory method that strongly focuses on the coupling mechanisms, but is not
very quantitative. However, it allows for disentangling the different mechanisms of action involved in coupling tropospheric
250　signals to the stratosphere without losing the involved timescales. Therefore, we correlate the geopotential as a function of
longitude, height and time with our precursor MSLP centres of action. Figure 7 illustrates the 10% largest absolute correlation
coefficients for the Ural region in November–February (NDJF). For better interpretation, we show three different views of
the same data — a three-dimensional view (left), a top view of tropospheric signals (≥200hPa, middle), and a top view of
stratospheric signals (<200hPa & ≥1hPa, right). The tropospheric response to MSLP changes in the Ural region is mainly
255　barotropic, i.e. high surface pressure in the Ural area is connected to higher geopotential heights above it and vice versa. This
signal reaches the tropopause without a time lag but is disconnected from the main stratospheric signals, which emerge east of
the Ural region and propagate west- and eastward throughout time. Thus, a high-pressure anomaly in the Ural area is connected
to positive stratospheric geopotential anomalies that are a clear indication of a weakened stratospheric polar vortex. The strong
positive correlation coefficients remain in the stratosphere for up to 55 days in ERA5 and 30 days in the ICON ensemble. We
260　identify the Plumb wave activity flux (cf. Fig. 6) as a crucial link between the tropospheric instantaneous reaction at 60°E and
the stratospheric response that originates at 170°E. Except for the smaller time lag, the ICON ensemble is in good agreement
with the ERA5 occurrence of strong regression coefficients in time and space.
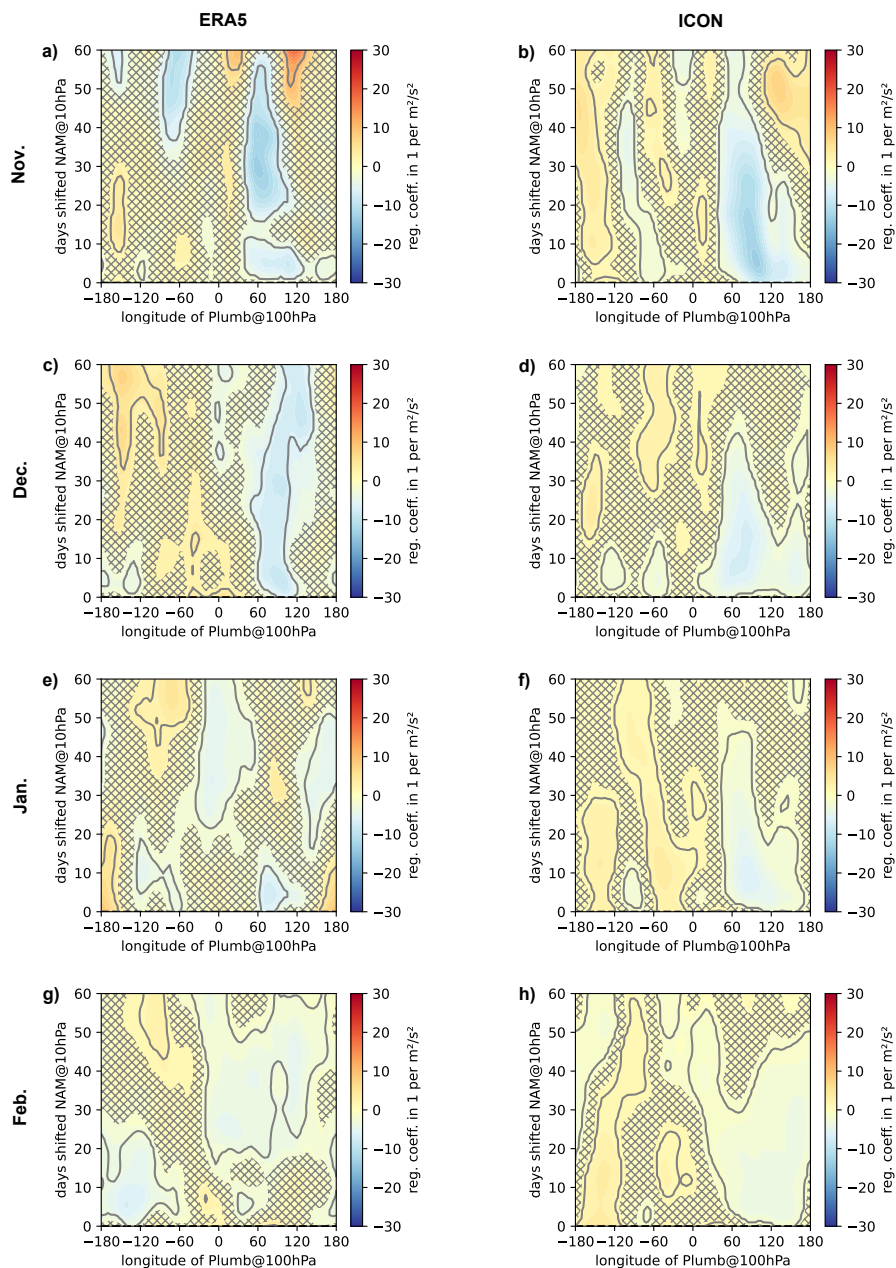
Figure 6. Regression of 45°N to 80°N meridional mean Plumb flux onto the 10 hPa NAM. The Plumb flux is averaged over 10° longitude bins with their respective center positions given along the x-axis. Daily values of Plumb flux from November (a,b), December (c,d), January (e,f) and February (g,h) of ERA5 data (a,c,e,g) and all years and ensemble members of ICON data (b,d,f,h) are used. Data of the 10 hPa NAM is shifted by days given on the y-axis relative to Plumb flux data. Areas with regression coefficients with p-values above 0.05 are hatched, areas with p-values below 0.001 are encircled.
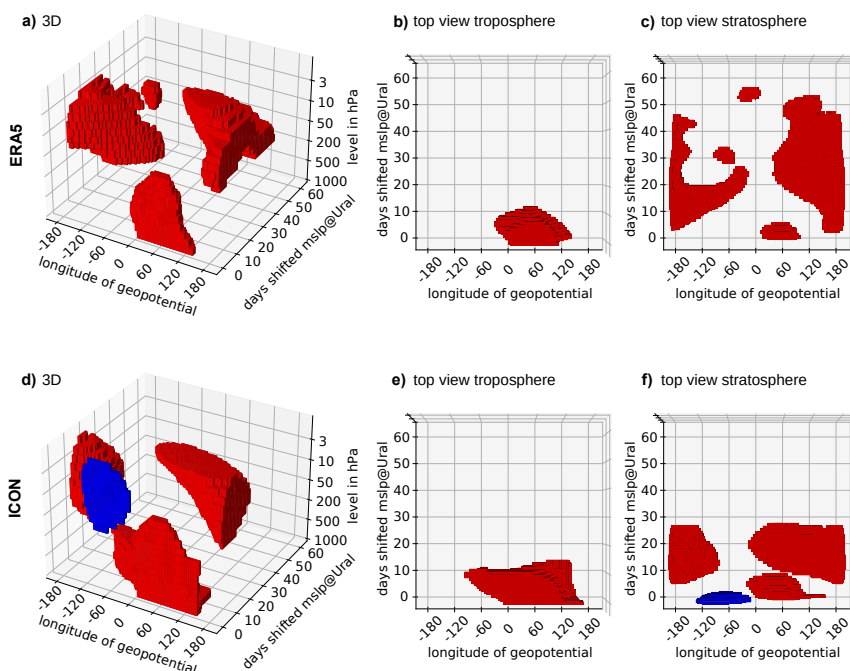
Figure 7. Correlation of the daily mean Ural (45°N–80°N and 30°E–100°E) MSLP in NDJF onto the daily, meridional mean geopotential (60°N–85°N) for ERA5 data (a-c) and the ICON ensemble (d-f). Figures a) and d) are a function of longitude [°], time [days], and height [hPa], whereas Figures b) and e) show a top view of tropospheric signals (≥200hPa) and Figures c) and f) show a top view of stratospheric signals (<200hPa & ≥1hPa). Only the 10% largest absolute correlation coefficients are shown, with red (blue) colours denoting a positive (negative) correlation.

For the extended Aleutian region, there is no clear indication that the Plumb flux plays a role in coupling the MSLP to the NAM (cf. Fig. 6). So what is the mechanism at play here? Figure 8 helps to answer this question: the Aleutian MSLP is

265 also positively correlated to the geopotential above it in the troposphere. However, it is additionally connected to a signal of the opposite sign that emerges at approximately 500 hPa and 80°W. This pattern resembles the two main centres of action of the PNA. It is this opposite signal which has a strong vertical structure and directly penetrates into the stratosphere. Hence, e.g. a low-pressure anomaly in the extended Aleutian low area is connected to positive geopotential anomalies in the mid-troposphere over North America, which directly penetrate into the stratosphere leading to a strengthening of the stratospheric

270 Aleutian High. This stratospheric pattern is strongly linked to a displacement of the stratospheric polar vortex towards Eurasia and the subsequent weakening of the NAM. A positive MSLP anomaly on the other hand would be connected to a more pole-centered, strong stratospheric polar vortex. The displacement character of the stratospheric response is reinforced by the opposite signal response towards Eurasia. The strong response in the stratospheric correlation coefficients to the Aleutian MSLP is less long-lasting than the Ural response — with up to 20 days in ERA5 and ICON. This is in agreement with the

275 overall weaker link between the extended Aleutian MSLP and stratospheric NAM compared to the Ural MSLP. Additionally, a
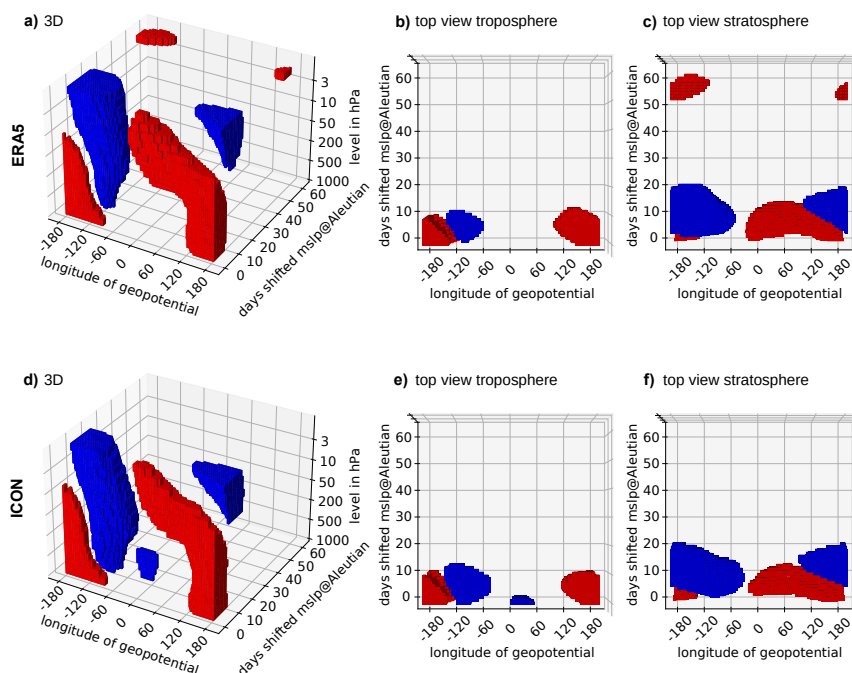
Figure 8. As in figure 7 but for the daily mean MSLP in the extended Aleutian area (45°N–80°N and 160°E–100°W).

displacement of the stratospheric polar vortex towards Eurasia could potentially allow for the Plumb flux from Ural anomalies to disturb the vortex, which would add to the improved predictability of the combined index. Overall, the reanalysis and model strongly agree on the processes of troposphere–stratosphere coupling for the extended Aleutian region.

4 Conclusions and discussion

280   This study conducts a comprehensive investigation of tropospheric precursors of stratospheric winter circulation by means of the NAM. Whereas part 3.1 of the results mainly focuses on the precursor patterns and involved timescales, part 3.2 investigates the involved coupling mechanisms. Based on the analysis of ERA5 reanalysis data and ICON ensemble simulations, the results from part 3.1 can be summarised as follows:

– We identify two main tropospheric precursor regions for stratospheric circulation in winter: the Ural area (45°N–80°N
285   and 30°E–100°E) and the extended Aleutian area (45°N–80°N and 160°E–100°W). Whereas the Ural MSLP exhibits significant negative regression coefficients, the extended Aleutian MSLP exhibits significant positive regression coefficients. I.e., a weak NAM is often preceded by high-pressure anomalies in the Ural area and/or low-pressure anomalies in the extended Aleutian area and vice versa.

- The timescales of these precursor patterns range from 5 to nearly 60 days, which strongly matches the timescales of subseasonal to seasonal prediction. The largest stratospheric predictability arises 25–45 prior in the Ural area and 20–30 days in the extended Aleutian area.

- A simple monthly mean precursor index based on the detrended MSLP differences between the Ural and the extended Aleutian area is strongly correlated to the NAM in 10 hPa of the following month. The strongest correlation is found between the December precursor index and January NAM at 10 hPa.

- Time–height development plots of the NAM for precursor composites additionally take into account the downward coupling from the stratosphere to the troposphere. The original anomaly in the precursor index is connected to significant surface influence in the following one to three months. Thus, once again highlighting the importance of coupling processes between the troposphere and stratosphere for seasonal prediction in mid-latitude winter.

The precursor patterns in our study match findings from earlier studies, in particular for the Ural region (e.g. Baldwin et al., 2021; Cohen and Jones, 2011; Garfinkel et al., 2010). Additionally, we were able to identify the involved timescales by not averaging over fixed lag times. Based on these precursor patterns, in Sect. 3.2 we investigated the involved coupling mechanisms and identified two different pathways for troposphere–stratosphere coupling:

- Vertical planetary wave propagation connects MSLP anomalies in the Ural area to the strength of the stratospheric NAM. The stratospheric polar vortex is particularly sensitive to the Plumb flux changes in the east of the Ural area, with lag times of up 60 days. Increased Plumb flux in this area is connected to a weakened stratospheric polar vortex. This relationship does not hold for other regions.

- Vertical planetary wave fluxes do not explain the link between extended Aleutian MSLP and the stratospheric NAM. Here it is a pattern that resembles the two main centres of action of the PNA which directly penetrates into the stratosphere. Whereas the Aleutian pressure anomaly remains in the troposphere mainly, it triggers an opposite pressure pattern in the mid-troposphere over North America. This reaches the stratosphere towards the Aleutian area. Hence, an intensified Aleutian Low in the troposphere is related to a strengthened Aleutian High in the stratosphere, which is connected to a displaced and weakened stratospheric polar vortex.

Overall, the results of this study highlight the potential of stratospheric processes for subseasonal to seasonal prediction. In agreement with Domeisen et al. (2020b) we demonstrate, that the timescales of upward troposphere–stratosphere coupling can exceed the deterministic range of weather prediction. However, in this study, we investigate the involved coupling mechanisms in a climatological sense, and the described precursor patterns, pathways and timescales can differ for each event. I.e. an analysis of single events shows that 20–25% of the strong/weak stratospheric vortex events are preceded by a precursor index that is not expected to trigger the given stratospheric anomaly. Thus, it is very important to mention that the bottom-up perspective based on Matsuno (1971) cannot explain the full variability of the stratospheric polar vortex, as also the current state and position of the stratospheric polar vortex plays a large role. E.g. Birner and Albers (2017) argue that approximately only one-third of sudden stratospheric vortex decelerations are preceded by extreme anomalous upward planetary wave fluxes.

Yet, we demonstrate that localised upward planetary wave fluxes cannot explain the full range of upward coupling between the troposphere and stratosphere, as vertical structures in the geopotential are able to directly penetrate into the stratosphere and push the vortex out of stability, a process that is particularly important for the Aleutian precursor pattern. In contrast

325 to Domeisen et al. (2019), our analysis does not suggest strengthened wave flux into the stratosphere in the Aleutian area during a deepened Aleutian Low. Moreover, fluxes in this region only have a very weak influence on the strength of the stratospheric polar vortex. This can be explained by the climatological position of the stratospheric polar vortex shifted towards Eurasia. Overall, this study emphasises the importance of the non-zonally-averaged picture for an in-depth understanding of troposphere–stratosphere coupling mechanisms. By using a time and space-resolved method this study offers a novel approach

330 to investigating pathways of troposphere–stratosphere coupling.

Moreover, this is the first study to show that upward troposphere–stratosphere coupling is realistically represented in ICON. In agreement with Köhler et al. (2021), we also demonstrate that the downward propagation of stratospheric anomalies back into the troposphere is realistically simulated in ICON. However, before the ICON model can make use of stratospheric processes for actual seasonal predictions, issues within the tropical stratosphere, in particular with the quasi-biennial oscillation

335 (Köhler et al., 2021), need to be solved. Nevertheless, the realistic representation of extratropical troposphere–stratosphere coupling in ICON is a first step towards using the atmosphere component of ICON for seasonal predictions in future.

References

Afargan-Gerstman, H. and Domeisen, D. I. V.: Pacific modulation of the North Atlantic storm track response to sudden stratospheric warming events, Geophys. Res. Lett.s, 47, e2019GL085 007, https://doi.org/10.1029/2019GL085007, 2020.

Baldwin, M. P. and Dunkerton, T. J.: Stratospheric harbingers of anomalous weather regimes, Science, 294, 581–584, https://doi.org/10.1126/science.1063315, 2001.

Baldwin, M. P. and Thompson, D. W. J.: A critical comparison of stratosphere–troposphere coupling indices, Quarterly Journal of the Royal Meteorological Society: A journal of the atmospheric sciences, applied meteorology and physical oceanography, 135, 1661–1672, https://doi.org/10.1002/qj.479, 2009.

Baldwin, M. P., Birner, T., Brasseur, G., Burrows, J., Butchart, N., Garcia, R., Geller, M., Gray, L., Hamilton, K., Harnik, N., et al.: 100 years of progress in understanding the stratosphere and mesosphere, Meteorological Monographs, 59, 27–1, https://doi.org/10.1175/AMSMONOGRAPHS-D-19-0003.1, 2019.

Baldwin, M. P., Ayarzagüena, B., Birner, T., Butchart, N., Butler, A. H., Charlton-Perez, A. J., Domeisen, D. I. V., Garfinkel, C. I., Garny, H., Gerber, E. P., et al.: Sudden stratospheric warmings, Reviews of Geophysics, 59, e2020RG000 708, https://doi.org/10.1029/2020RG000708, 2021.

Bao, M., Tan, X., Hartmann, D. L., and Ceppi, P.: Classifying the tropospheric precursor patterns of sudden stratospheric warmings, Geophysical Research Letters, 44, 8011–8016, https://doi.org/10.1002/2017GL074611, 2017.

Bauer, D. F.: Constructing confidence sets using rank statistics, Journal of the American Statistical Association, 67, 687–690, https://doi.org/10.2307/2284469, 1972.

Birner, T. and Albers, J. R.: Sudden stratospheric warmings and anomalous upward wave activity flux, Sola, 13, 8–12, https://doi.org/10.2151/sola.13A-002, 2017.

Blackmon, M. L. and Lau, N.-C.: Regional characteristics of the Northern Hemisphere wintertime circulation: A comparison of the simulation of a GFDL general circulation model with observations, Journal of the Atmospheric Sciences, 37, 497–514, https://doi.org/10.1175/1520-0469(1980)037<0497:RCOTNH>2.0.CO;2, 1980.

Butchart, N.: The stratosphere: a review of the dynamics and variability, Weather and Climate Dynamics, 3, 1237–1272, https://doi.org/10.5194/wcd-3-1237-2022, 2022.

Charlton-Perez, A. J., Ferranti, L., and Lee, R. W.: The influence of the stratospheric state on North Atlantic weather regimes, Quarterly Journal of the Royal Meteorological Society, 144, 1140–1151, https://doi.org/10.1002/qj.3280, 2018.

Cohen, J. and Jones, J.: Tropospheric precursors and stratospheric warmings, Journal of climate, 24, 6562–6572, https://doi.org/10.1175/2011JCLI4160.1, 2011.

Cohen, J., Zhang, X., Francis, J., Jung, T., Kwok, R., Overland, J., Ballinger, T. J., Bhatt, U. S., Chen, H. W., Coumou, D., et al.: Divergent consensuses on Arctic amplification influence on midlatitude severe winter weather, Nature Climate Change, 10, 20–29, https://doi.org/10.1038/s41558-019-0662-y, 2020.

Crasemann, B., Handorf, D., Jaiser, R., Dethloff, K., Nakamura, T., Ukita, J., and Yamazaki, K.: Can preferred atmospheric circulation patterns over the North-Atlantic-Eurasian region be associated with arctic sea ice loss?, Polar Science, 14, 9–20, https://doi.org/10.1016/j.polar.2017.09.002, 2017.

Domeisen, D. I., Garfinkel, C. I., and Butler, A. H.: The teleconnection of El Niño Southern Oscillation to the stratosphere, Reviews of Geophysics, 57, 5–47, https://doi.org/10.1029/2018RG000596, 2019.

Domeisen, D. I. V., Butler, A. H., Charlton-Perez, A. J., Ayarzagüena, B., Baldwin, M. P., Dunn-Sigouin, E., Furtado, J. C., Garfinkel, C. I., Hitchcock, P., Karpechko, A. Y., et al.: The role of the stratosphere in subseasonal to seasonal prediction: 2. Predictability arising from

395   stratosphere-troposphere coupling, J. Geophys. Res.: Atmospheres, 125, e2019JD030 923, https://doi.org/10.1029/2019JD030920, 2020a.

Domeisen, D. I. V., Butler, A. H., Charlton-Perez, A. J., Ayarzagüena, B., Baldwin, M. P., Dunn-Sigouin, E., Furtado, J. C., Garfinkel, C. I., Hitchcock, P., Karpechko, A. Y., et al.: The Role of the Stratosphere in Subseasonal to Seasonal Prediction: 1. Predictability of the Stratosphere, Journal of Geophysical Research: Atmospheres, 125, e2019JD030 920, https://doi.org/10.1029/2019JD030920, 2020b.

Durack, P. J. and Taylor, K. E.: PCMDI AMIP SST and sea-ice boundary conditions version 1.1.4,

400   https://doi.org/10.22033/ESGF/input4MIPs.2204, 2018.

Garfinkel, C. I., Hartmann, D. L., and Sassi, F.: Tropospheric precursors of anomalous Northern Hemisphere stratospheric polar vortices, Journal of Climate, 23, 3282–3299, https://doi.org/10.1175/2010JCLI3010.1, 2010.

Hersbach, H., Bell, B., Berrisford, P., Hirahara, S., Horányi, A., Muñoz-Sabater, J., Nicolas, J., Peubey, C., Radu, R., Schepers, D., et al.: The ERA5 global reanalysis, Quarterly Journal of the Royal Meteorological Society, 146, 1999–2049, https://doi.org/10.1002/qj.3803, 2020.

405 Hollander, M., Wolfe, D. A., and Chicken, E.: Nonparametric statistical methods, vol. 751, John Wiley & Sons, 2013.

Hoshi, K., Ukita, J., Honda, M., Nakamura, T., Yamazaki, K., Miyoshi, Y., and Jaiser, R.: Weak stratospheric polar vortex events modulated by the Arctic sea-ice loss, Journal of Geophysical Research: Atmospheres, 124, 858–869, https://doi.org/10.1029/2018JD029222, 2019.

Jaiser, R., Nakamura, T., Handorf, D., Dethloff, K., Ukita, J., and Yamazaki, K.: Atmospheric winter response to Arctic sea ice changes in reanalysis data and model simulations, Journal of Geophysical Research: Atmospheres, 121, 7564–7577,

410   https://doi.org/10.1002/2015JD024679, 2016.

Jaiser, R., Akperov, M., Timazhev, A., Romanowsky, E., Handorf, D., and Mokhov, I.: Linkages between Arctic and Mid-Latitude Weather and Climate: Unraveling the Impact of Changing Sea Ice and Sea Surface Temperatures during Winter, Meteorologische Zeitschrift, https://doi.org/10.1127/metz/2023/1154, 2023.

Karpechko, A. Y.: Predictability of sudden stratospheric warmings in the ECMWF extended-range forecast system, Monthly Weather Review,

415   146, 1063–1075, https://doi.org/10.1175/MWR-D-17-0317.1, 2018.

Köhler, R., Handorf, D., Jaiser, R., Dethloff, K., Zängl, G., Majewski, D., and Rex, M.: Improved Circulation in the Northern Hemisphere by Adjusting Gravity Wave Drag Parameterizations in Seasonal Experiments With ICON-NWP, Earth and Space Science, 8, e2021EA001 676, https://doi.org/10.1029/2021EA001676, 2021.

Kretschmer, M., Runge, J., and Coumou, D.: Early prediction of extreme stratospheric polar vortex states based on causal precursors,

420   Geophysical research letters, 44, 8592–8600, https://doi.org/10.1002/2017GL074696, 2017.

Matsuno, T.: A dynamical model of the stratospheric sudden warming, Journal of Atmospheric Sciences, 28, 1479–1494, https://doi.org/10.1175/1520-0469(1971)028<1479:ADMOTS>2.0.CO;2, 1971.

Overland, J. E., Dethloff, K., Francis, J. A., Hall, R. J., Hanna, E., Kim, S.-J., Screen, J. A., Shepherd, T. G., and Vihma, T.: Nonlinear response of mid-latitude weather to the changing Arctic, Nature Climate Change, 6, 992–999, https://doi.org/doi.org/10.1038/nclimate312, 2016.

425 Plumb, R. A.: On the three-dimensional propagation of stationary waves, Journal of Atmospheric Sciences, 42, 217–229, https://doi.org/10.1175/1520-0469(1985)042<0217:OTTDPO>2.0.CO;2, 1985.

Scaife, A. A., Karpechko, A. Y., Baldwin, M. P., Brookshaw, A., Butler, A. H., Eade, R., Gordon, M., MacLachlan, C., Martin, N., Dunstone, N., et al.: Seasonal winter forecasts and the stratosphere, Atmospheric Science Letters, 17, 51–56, https://doi.org/10.1002/asl.598, 2016.

Siew, P. Y. F., Li, C., Sobolowski, S. P., and King, M. P.: Intermittency of Arctic–mid-latitude teleconnections: stratospheric pathway between autumn sea ice and the winter North Atlantic Oscillation, Weather and Climate Dynamics, 1, 261–275, https://doi.org/10.5194/wcd-1-261-2020, 2020.

Wald, A.: Tests of statistical hypotheses concerning several parameters when the number of observations is large, Transactions of the American Mathematical society, 54, 426–482, 1943.

Zängl, G., Reinert, D., Rípodas, P., and Baldauf, M.: The ICON (ICOsahedral Non-hydrostatic) modelling framework of DWD and MPI-M: Description of the non-hydrostatic dynamical core, Quarterly Journal of the Royal Meteorological Society, 141, 563–579, https://doi.org/https://doi.org/10.1002/qj.2378, 2015.